V International Conference on Computational Methods in Marine Engineering
MARINE 2013
B. Brinkmann and P. Wriggers (Eds)

NUMERICAL PREDICTION OF THE PERFORMANCE OF AXIAL-FLOW HYDROKINETIC TURBINE

PAVAN CHANDRAS[1], LAVEENA SHARMA[2] AND DHIMAN CHATTERJEE[3]

Department of Mechanical Engineering,
Indian Institute of Technology Madras,
Chennai, TamilNadu, INDIA.
1. e-mail: chandraspavan@gmail.com
2. e-mail: sharma.laveena071@gmail.com
3. email: dhiman@iitm.ac.in

Key words: Hydrokinetic Turbine, Numerical Simulation, Performance, Geometry, Free Surface

Abstract. *The present work is focused on the numerical prediction of the performance of axial flow hydrokinetic turbine under practical conditions. The models are designed to produce an electrical power output of 200 W at an incoming water speed of 1 m/s. Three different models of three-bladed turbine, based on swept direction, are designed to study the effect of geometry on the turbine performance while operating under identical conditions. Numerical simulations indicate that a peak turbine power of 480 W at a tip speed ratio of 3.5 is obtained for unswept bladed turbine with sharp trailing edge. Results suggest that forward and backward swept blades perform better than the unswept blade for blunt trailing edge. Simulations are carried out for different nose profiles for hub. It is found that a turbine experiences lesser thrust force with an ellipsoidal nose having ratio of major axis to minor axis of 4. In order to capture a real life scenario effectively, the effect of turbine location inside the water, particularly with respect to the free surface is investigated further. The safe depth for turbine installation is found to be at least 1.4 m from the free surface.*

1 INTRODUCTION

Hydrokinetic turbine, utilizing kinetic energy of flowing water, offers a renewable source of extracting power from rivers and seas. Though this type of "net-zero head" turbine has lower efficiency than conventional dam-dependent hydraulic turbine, yet this is more suited from the perspective of minimum adverse effect on environment and population displacement. Hence, there is a spurt in research activities in studying these turbines [1].

These types of turbines can be axial-flow or cross-flow depending on the disposition of the shaft with respect to the flowing water current. Axial-flow hydrokinetic turbine, the focus of present work, has an axis of shaft parallel to the incoming flow while cross-flow turbine has axis perpendicular to the flow. Former is more efficient than later type of turbines but suffers from lower conversion efficiency in case the incoming flow direction does not match with the shaft direction. In such a scenario, use of properly designed ducts can prove to be beneficial [2, 3].

Practical works on the generation of electric power using axial-flow hydrokinetic turbine was done mainly by different industries [4-6]. However, with passage of time and with improvement in computational resource over the years, more and more papers are published

which predicts performance of these hydrokinetic turbines numerically [7, 8]. This shift towards numerical prediction also took place because numerical methods provide a quicker route to arrive at improved design. Sophisticated mathematical techniques like large eddy simulations to assess role of turbulence on turbine performance and resultant wake flow is used [7]. This approach being computationally resource intensive, many researchers resort to RANS for prediction of performance of hydrokinetic turbine [8]. Hence similar strategy of using RANS is adopted in the present work.

Present work discusses the design aspect of an axial-flow hydrokinetic turbine and its performance capability of the turbine as a function of tip speed ratio, incoming water speed and flow directions, as well as installation parameters like elevation from the river bed and depth from the free surface.

2 TURBINE DESIGN AND MODELLING

An axial-flow hydrokinetic turbine is designed to produce an electrical output power of 200 W. Generator efficiency (η_G) for these turbines running at low rotational speeds is expected to be low and hence it is taken to be 60%. A survey of existing designs indicates that, though Betz's limit is 59.3%, most of the turbines operate with much lower efficiencies. So, as a conservative estimate, turbine efficiency (expressed as power coefficient, C_p) is considered to be 35% in this work. Designing of the turbine is represented here in terms of design of rotor, hub and shaft.

2.1 Design of rotor blades

Electrical output power (P_{elec}) produced by a hydrokinetic turbine is given by the relation [9]:

$$P_{elec} = \frac{1}{2}\rho A V_{\infty}^{3} C_p \eta_G \tag{1}$$

In this equation, V_∞ is freestream (water current) speed much ahead of the turbine inlet and is taken in the present work to be 1 m/s unless specifically mentioned. ρ is the density of water and is taken as 997 kg/m^3. A is the projected area of the turbine. This relation yields tip diameter of the turbine (D_{tip}) to be 0.8 m. Various hub to tip ratios (D_{hub}/D_{tip}) were attempted, starting from high values of 0.35 to values as low values as 0.15. It was seen that higher ratios yielded poor performance while too low ratio may be unusable from stress (due to bending moment of long blades) considerations. Hence, hub diameter (D_{hub}) was taken as 0.3 m.

Based on the suggestion by Anyi and Kirke [10], we have also used S822 aerofoil as blade profile. As reported in that paper, other than improved stall characteristics and high lift to drag ratio it offers resistance against fouling. Figure 1(a) shows a typical S822 profile. Basic simulations were performed with this profile of the blade after choosing a desired angle of incidence of 5° at all locations from hub to tip as the profile shows high lift and low drag-lift ratio at this angle of attack. But from fabrication considerations, sharp trailing edge may not be realized in practice and hence after defining optimum parameters, later simulations to investigate the effect of sweep on blade performance were carried out using modified trailing edge with small but finite radius as shown in Figure 1(b).

The blade consists of nine stations, thicker at the root for greater flexural strength and narrower at the tip for minimum drag. Hence, the chord length of the blade airfoil gradually decreases from root to tip whereas the twist angles increases towards root. The blade is twisted with different twist angles in such a fashion that the relative speed of water (W) at every cross section gives rise to maximum lift by keeping the angle of attack reasonably constant throughout the blade span [10].

2.2 Design of hub

Hub geometry was modeled in Solid Works^{TM} with different nose profiles. Two types of configurations were modeled: hub with hemispherical front and rear, and hub with elliptical front and hemispherical rear (Fig. 2), to study the effect of hub geometry on the wake region as well as on the overall thrust force experienced by the turbine. Various ellipsoids with ratio of major axis to minor axis from 1 to 4 were tried out to check the reduction in thrust force with the ratio. This will be discussed later in the paper with simulated results.

2.3 Design of shaft

The diameter of the output shaft is designed to withstand the torque generated by the turbine at free stream water speed. With appropriate factor of safety and using steel as shaft material, shaft diameter was determined to be 50mm.

2.4 Blade Configurations

In this work, individual blade profiles at different radial locations stacked along their mid-chord, quarter-chord and along the leading edge to investigate the effect of sweep. Nine blade profiles from root to tip stacked along an axis joining the center of the airfoil chords leads to the construction of radial, unswept blades. While the profiles stacked from quarter chord i.e. 1/4th the chord length taken from leading edge results in backward sweep. The third one was stacked along the leading edge exactly like wind turbine blade profiles. This configuration gives rise to forward swept blades. Different blade configurations thus obtained are shown in Fig. 3.

3 GOVERNING EQUATION AND NUMERICAL TECHNIQUES

Turbulent, incompressible flow simulations were carried out using Reynolds-averaged Navier Stokes (RANS) equations based on equations described below [8]:

$$\nabla \bullet \vec{W} = 0$$

$$\rho\left[\frac{\partial \vec{W}}{\partial t} + \nabla \bullet \left(\vec{W}\vec{W}\right) + \left(2\vec{\Omega} \times \vec{W} + \vec{W} \times \vec{W} \times \vec{r}\right)\right] = -\nabla p + \nabla \bullet \tau \tag{2}$$

In this work, k-ω SST (Shear Stress Transport) turbulence model was chosen as it provides a good compromise between computational cost and solution accuracy for flows with swirl [8].

3.1 Numerical strategy

As already mentioned, solid model of the turbine geometry was created in Solid Works^{TM}. Meshing was done in ICEMCFD^{TM} while numerical simulations were carried out using ANSYS CFX^{TM}.

The computational domain consists of far field which is non-rotating, while the rotor domain rotates at the rotational speed of turbine. Inlet condition is specified in terms of freestream velocity (V_∞), outlet boundary is depicted as pressure boundary condition (Fig. 4). Fine structured mesh is created for the rotor using grid generating tool, TurboGrid^{TM}. For simplicity, unstructured mesh is created for far field domain in ICEM CFD. For most of the work reported here, exchange of pressure and velocity data across stationary and rotating frames of references were carried out using frozen rotor method. Though this model cannot capture transient effects at the interface, yet it offers steady state solutions to multiple frames of reference problem. This approach was adopted as it is computationally less expensive. In problems dealing with free-surface, transient analysis was carried out and for those cases only, frozen rotor interaction was replaced by transient rotor-stator interaction. Flowchart indicating sequence of operations adopted is given in Fig. 5 for clarity. Second-order advection schemes were used for numerical simulations in order to minimize numerical diffusion. Convergence control is performed in terms of physical timescale, which in this case is defined as the inverse of rotational speed [rad/s] of rotor.

To establish the credibility of the numerical results, a domain independence study, a grid sensitivity study and a study on rms-residuals was carried out. These are now taken up for discussion.

3.2 Domain independence study

Ideally far-field domain should be made as large as possible. However, too large a computational domain is computationally expensive and may not contribute to accuracy of the predictions. Hence, the study was conducted for three separate far-field domains - small, medium and large on the basis of their volume. The idea here is to choose a domain which can offer result that matches with the ideal trend obeyed by the turbines, and in minimum run time. Table 1 summarizes the effort in this direction and enables us to choose appropriate computational domain. The far field domain is made cylindrical whose diameter is taken as 5 times the diameter of the rotor tip and is extended $3D_{tip}$ upstream and $7D_{tip}$ downstream to negate any undesirable boundary effects thereby offering a good trade-off between reliability of results and computational effort.

3.3 Grid sensitivity study

Grid sensitivity study was carried out to determine the effect of mesh sizes on the predicted turbine performance. It was seen that grid independent solution was obtained for a mesh having 22,09,641 number of nodes in the rotating domain along with 3,86,972 nodes in the stator. Hence this mesh was adopted for the present work.

3.4 Study on RMS residuals

Effect of fixing the convergence level may have significant effect on the performance of

the turbine. For industrial applications, ANSYS CFX recommends a rms convergence level of 10^{-4}. We have tried to ascertain the influence of results obtained with by computing for a rms level of 10^{-5}. Outcome of such study indicates that for present computations 10^{-4} residual level suffices.

Table 1 Comparison between results of various far-field domains

Property	Small	Medium	Large
Volume of far field (x149.158 m^3)	1 (D X L)	3.37 (1.5D X 1.5L)	11.37 (2.25D X 2.25L)
No. of nodes in far field domain	1,90,710	3,86,972	10,88,203
Power coefficient	0.51	0.49	0.49
Percentage difference in results	3.9 %	0.8 %	-
Run time of simulation	3 hr 22min	3hr 39min	7hr 20 min

Thus after having ascertained different parameters that may affect the outcome of numerical prediction, we now present the significant results.

4. RESULTS AND DISCUSSION

Figure 6(a) depicts the variation of static pressure along the flow direction. This plot proves the capability of numerical simulations to capture the essential flow physics. It is observed that the rotor slows the water speed of 1 m/s far upstream to 0.65 m/s at the plane of rotation due to drag which develops from the pressure drop over the rotor. This pressure drop depends on the water density and viscosity, initial water speed, and final water speed at the rotor plane. A small pressure rise is expected upstream of the rotor before a discontinuous pressure drop over the rotor. During the downstream action of the rotor, the pressure returns continuously to the atmospheric level while the flow regains velocity. However, unlike classical actuator disc theory, the rotor imparts a rotational velocity as can be seen from the streamlines in the wake of the turbine (Fig. 6b).

Figure 7 depicts predicted turbine output power for different rotational speeds. It is seen that there is a peak in output power at around 42 rpm corresponding to a tip speed ratio (λ) of 3.5 which is quite close to the selected design condition of λ =4. To understand what happens at lower or higher values of tip speed ratio, Fig. 8 shows streamlines past the blade at mid-span. It shows that at lower tip-speed ratios like 2, there is a large-scale flow separation indicative of stall, resulting in lower lift to drag ratio and hence lower power output. At higher tip-speed ratio of 6, the flow incidence angle is close to zero, resulting in low pressure difference between pressure and suction sides — thereby giving rise to very low lift value.

4.1 Performance at various incoming speed

The incoming flow water speed in river or seas need not remain constant in natural conditions. Hence, similar simulations were conducted to compute the variation of power coefficient (C_p) with tip speed ratio (λ) as a function of incoming water speed. Figure 9(a) shows variation of power coefficient with different tip speed ratios. On the other hand, power output should increase as cubic power of speed of incoming water flow. Figure 9(b) shows the variation and power-law curve fitting indicates that $P_c = 491.5V_\infty^{3.03}$ with $R^2 = 1$.

4.2 Performance at different flow directions

Hydrokinetic turbines, utilizing water currents, are affected by variation in flow directions. It is also known that axial-flow machines are more susceptible to this phenomenon. So, numerical simulations were carried out to determine the variation of power coefficient at different tip speed ratios as a function of incoming flow directions ranging from 0^o to 20^o (Fig. 10). It is seen that, as the flow deviates from the axis, performance deteriorates and for 20^o of deviation, peak power coefficient drops from 0.48 to 0.42 at tip speed ratio of 3. As the angle of approach progresses, the effect of flow separation becomes more pronounced and results in the drop in efficiency of the turbine.

4.3 Effect of hub geometry on turbine performance

The airfoil is designed to offer maximum lift to make the rotor revolve, with minimum drag. Combination of these forces result in tangential force and axial and radial thrust. The tangential force provides necessary torque. The thrust force perpendicular to the plane of rotation is undesirable. Our work suggests that thrust variation could result from the shape of the hub while power coefficient is largely unaffected by changes in hub profile (Fig. 11). The variation of thrust is plotted as a function of nose profile defined by the ratio of major axis to minor axis, ranging from 1 to 4. A reduction in the thrust force with increase in ratio is observed here. It is important to note here, hub nose profile has an impact over thrust but does not show any considerable effect on the power coefficient. This reduction can be explained in terms of pressure gradient across the hub and the expansion of wake in the surrounding region. Out of the designed configurations hub with hemispherical front and rear offers sudden pressure rise while on the other hand, hub with ellipsoidal front displays a smooth rise in pressure throughout the span.

4.4 Performance at various elevations from river bed

The flow speed of water in a river varies from the river bed to free surface. Hence, the performance of the turbine was studied at various elevations from river bed assuming linear variation of water speed of 0 to 2 m/s from bottom to free surface. Assuming depth of river to be 10m, output power and thrust force are plotted against elevations ranging from 2m to 5m (Fig. 12).

It should be noted here that the effect of relative angular position of the blades at different incoming flow directions with different elevations is not accounted here. Transient simulations are needed to plot the torque values as a function of both varying incoming speed and varying incoming flow directions taken together. Therefore, simulations to plot torque

against different angular positions at different elevations were carried out separately, taking identical velocity profile from top to bottom.

Though that numerical analysis indicates that the rate of increase in output power with respect to elevation is significantly higher than that of thrust force, we cannot afford to mount the turbine beyond certain height. This is because, the bending moment of the supporting tower increases at a higher rate, due to the combined effect of height and the thrust force. The height at which turbine should be mounted can be calculated only after fixing the geometrical shape and material of the tower, which is beyond the scope of this study.

4.5 Safe depth below the free surface

Simulations done to determine how the performance of this turbine gets affected in the presence of free surface indicate that if the turbine is not mounted at a safe depth, the free surface may interact with the rotating turbine thereby causing a dip in the free surface due to sudden drop in pressure below the atmospheric pressure as the flow past the rotor.

Furthermore, if the effect of free-surface becomes significant, the usual scaling law of same blade-based Reynolds number and turbomachines relations will not be valid for the existing turbine. Froude number ($Fr = V_{rel,tip} \Big/ \sqrt{gH_{depth}}$) can be used to determine the free surface interaction with the rotating blades. Here, the characteristic velocity of flow is taken as the relative velocity at the tip of the rotating blade which is the maximum speed observed. The characteristic length (H_{depth}) is chosen as the distance from axis of rotation of turbine to the free surface. Taking Froude number as 0.95, for subcritical flow regime, the safe depth at which the turbine may be mounted is calculated as 1.4 m. Figure 13 shows typical contour of vapour fraction of water indicating the location of free surface.

4.6 Effect of blunt trailing edge

Figure 14 indicates the variation of power coefficient with tip-speed ratio for unswept rotor with and without blunt trailing edges. It is clear from Fig. 8 that there is degradation in turbine performance which could be due to the blunt trailing edge that causes flow separation downstream of the trailing edge.

4.7 Effect of blade sweep

Blade sweep, as discussed earlier, was attempted as it is well known that sweeping of turbine blades in turbomachine applications can influence the performance of the machine. It may be noted here that the results shown in Fig. 15 are for these three configurations with blunt trailing edges. Among these unswept blade is the worst in terms of performance though the behaviour is similar. Hence, results discussed so far on unswept blade is expected to be valid for swept blades as well.

5 CONCLUSION

Numerical prediction of hydrokinetic turbine performance was carried out and it was demonstrated that an ellipsoidal hub shape can reduce thrust without compromising on the performance. Different blade sweeps were achieved through stacking of blades along different chord locations and it was seen that the performance of forward swept blade is the best (with

shaft power of 385 W) and unswept blade performs worst (shaft power of 373 W). Blunt trailing edge, necessitated from manufacturing constraints, reduces performance of the turbine when compared with that due to sharp trailing edge. Effect of turbine location inside the water body seems to affect the turbine performance and care must be taken to have appropriate depth below the water-air interface. From the present results, a safe depth of 1.4 m below the free surface for the given turbine configurations was shown to be necessary.

ACKNOWLEDGEMENT

Authors would like to acknowledge the funding received from National Institute of Ocean Technology, Chennai, India.

REFERENCES

[1] Khan M.J., Bhuyan G, Iqbal M.T., Quaicoe J.E. Hydrokinetic energy conversion systems and assessment of horizontal and vertical axis turbines for river and tidal applications: a technology status review. *Applied Energy* (2009) **86**:1823-1835.

[2] Malipeddi, A. R. and Chatterjee, D. Influence of duct geometry on the performance of Darrieus hydroturbine. *Renewable Energy* (2012) **43**, 292-300.

[3] Setoguchi T. Development of two-way diffuser for fluid energy conversion system. *Renewable Energy* (2004) **29(10)**1757-1771.

[4] http://verdantpower.com

[5] http://www.bluenergy.com/Technology.htm

[6] http://www.gcktechnology.com/GCK/pg2.html

[7] Kang, S., Borazjani, I., Jonathan, A.C. and Sotiropoulos, F. Numerical simulation of 3D flow past a real-life marine hydrokinetic turbine. *Adv. Water Res.* (2012) **39**, 33–43.

[8] Mukherji, S. S. Kolekar, N., Banerjee, A. and Mishra, R. Numerical investigation and evaluation of optimum hydrodynamic performance of a horizontal axis hydrokinetic turbine. *J. Renewable Sustainable Energy* (2011) **3**, 063105.

[9] Guney, M. S. and. Kaygusuz, K. Hydrokinetic energy conversion systems: A technology status review. *Renewable and Sustainable Energy Reviews* (2010) **14**, 2996–3004.

[10] Anyi, M. and Kirke, B. Hydrokinetic turbine blades: Design and local construction techniques for remote communities. *Energy for Sustainable Development* (2011) **15**, 223-230.

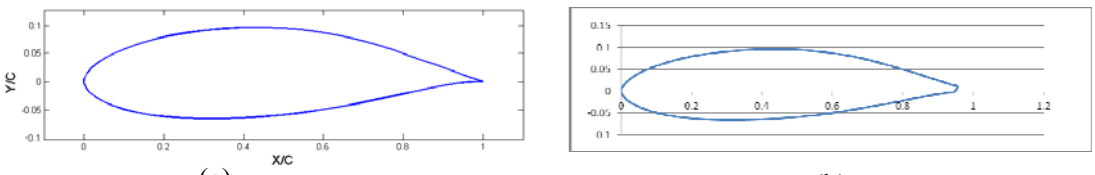

(a) (b)

Figure 1. Profiles of S822: a) original profile, b) modified profile

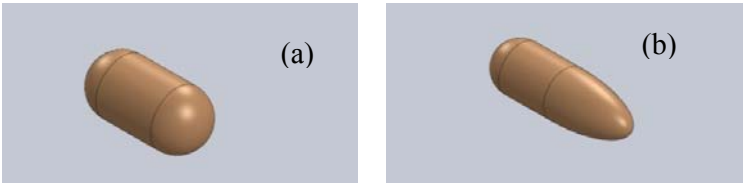

Figure 2. Profiles of hub: a) hemispherical front b) ellipsoidal front

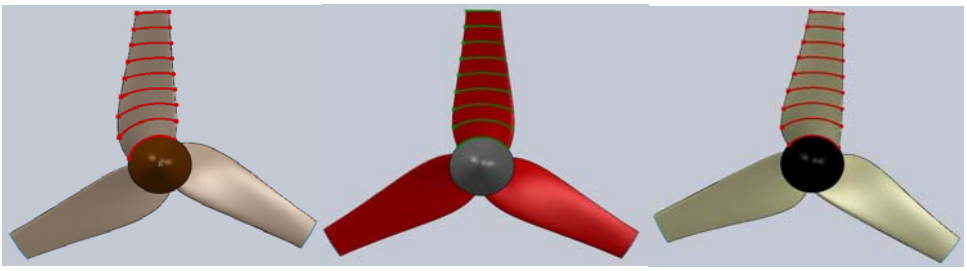

Figure 3. Front views of (a) backward-swept, (b) zero swept, and, (c) forward-swept turbine geometries

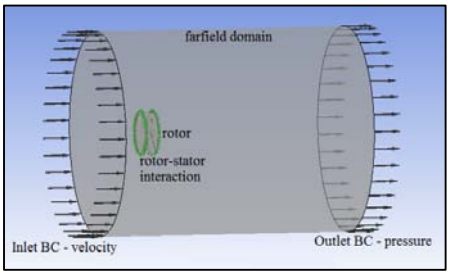

Figure 4. Computational domain along with boundary conditions

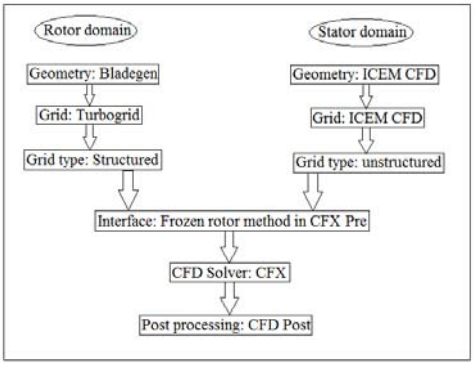

Figure 5. Numerical strategy adopted in predicting hydrokinetic turbine performance

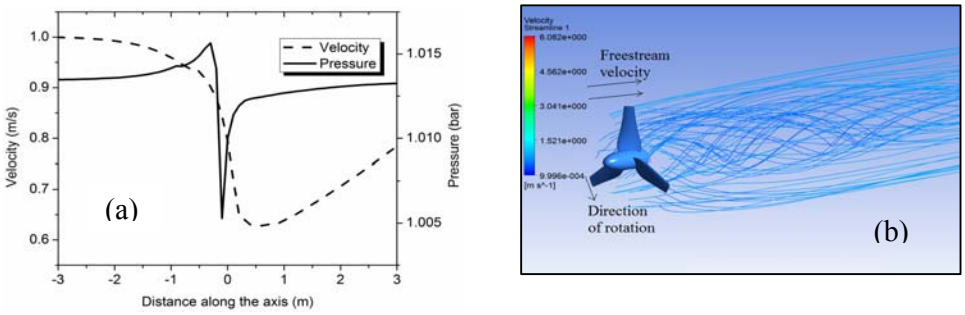

Figure 6. (a) Pressure and velocity variation axial direction, (b) Streamlines in the wake of rotating turbine

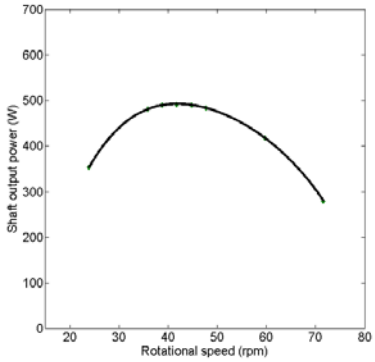

Figure 7. Variation of shaft out power with rotational speed

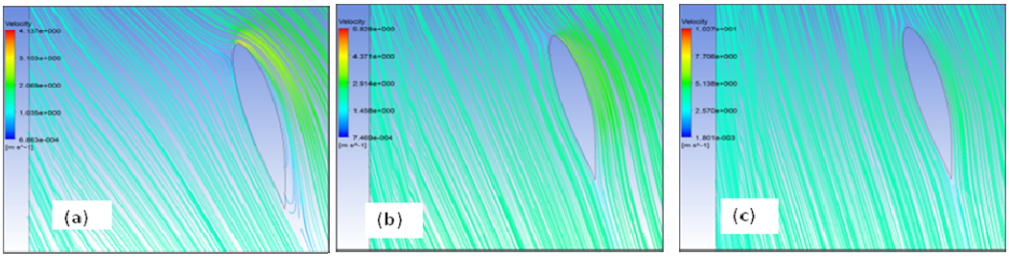

Figure 8. Streamlines depicting relative velocity near a blade at mid-span. (a) λ=2, (b) λ=3.5 and (c) λ=6

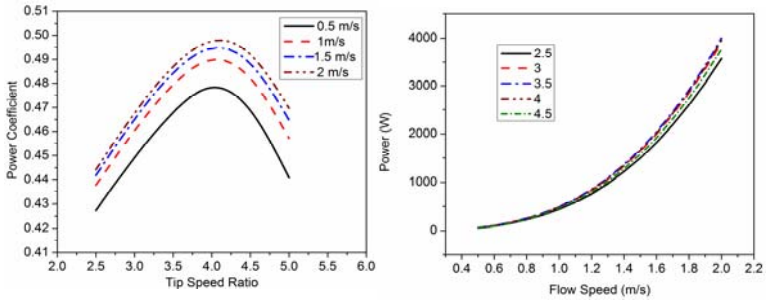

Figure 9. Effect of freestream speed. (a) Variation of power coefficient with tip speed ratio and (b) Variation of maximum output power with freestream speed

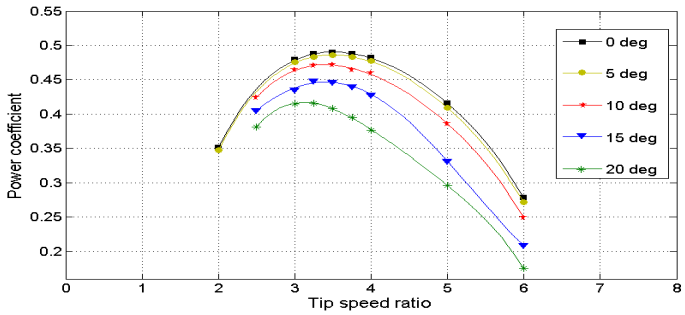

Figure 10. (a) Effect of incoming flow direction on turbine performance

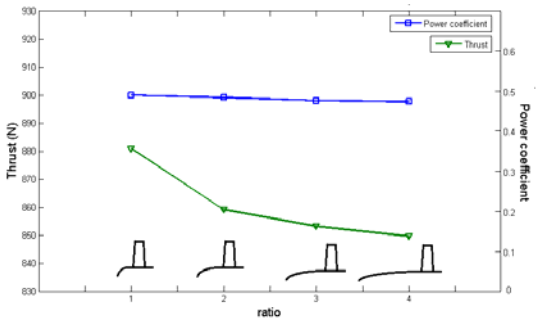

Figure 11. Effect of nose profile on thrust and power coefficient

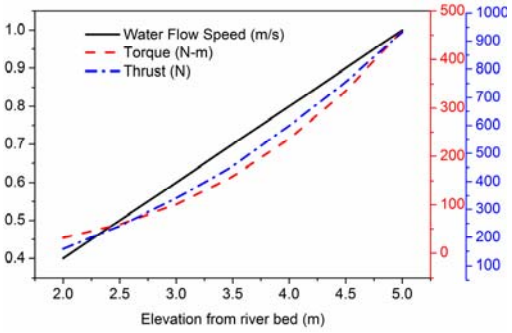

Figure 12. Effect of elevation on turbine performance

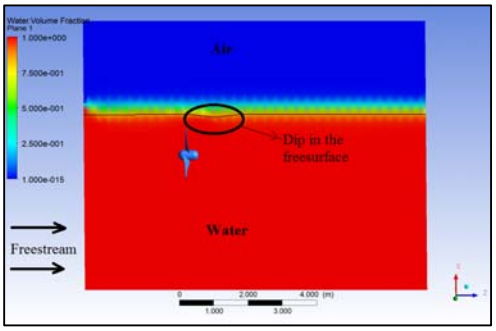

Figure 13. Variation of free surface height due to the placement of turbine near the surface

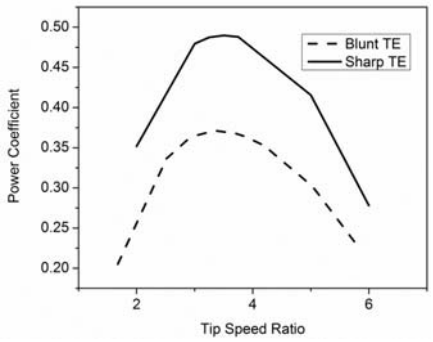

Figure 14. Effect of trailing edge shape on turbine performance

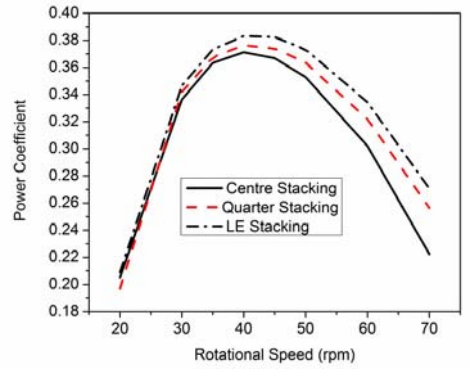

Figure 15. Effect of blade stacking and orientation on turbine performance